LATERAL RESISTANCE OF A SHORT RIGID PILE IN A TWO-LAYER COHESIONLESS SOIL

ERDAL UNCUOĞLU IN MUSTAFA LAMAN

about the authors

corresponding author
Erdal Uncuoğlu
Erciyes University,
Civil Engineering Department
38039 Talas / Kayseri, Turkey
E-mail: erdalu@erciyes.edu.tr

Mustafa Laman
Osmaniye Korkut Ata University,
Civil Engineering Department
80000, Osmaniye, Turkey
E-mail: mustafalaman@osmaniye.edu.tr

abstract

The behavior of a laterally loaded short rigid pile founded in a two-layer sand soil profile has been investigated. For this purpose, a series of model tests were carried out on model piles. The effects of the elasticity modulus, dilatancy and interface behavior of the sand have been explored numerically by performing a series of three-dimensional non-linear finite-element analyses. The lateral load capacities in the layered sand conditions have been calculated using the methods proposed by Brinch Hansen (1961) and Meyerhof et al. (1981). The results obtained from experimental studies, numerical analyses and a conventional method were compared with each other. The results proved that the parameters investigated had a considerable effect on the behavior of short rigid piles subjected to lateral loads. It was also shown that the value of the ultimate lateral load capacity could vary significantly, depending on the methods used.

keywords

lateral load, short pile, two-layered sand, model test, finite element, lateral effective stress

1 INTRODUCTION

Short piles or pier foundations that have a large diameter are widely used to support structures such as transmission towers, advertisement and information posts, overhead catenary systems carrying electrical power in railway networks and water towers. These structures have to withstand significant lateral loads and overturning moments, but relatively small vertical forces, which as a consequence are often neglected.

The behavior of piles subjected to lateral loads is governed by the interaction between the pile and the soil, and it is a non-linear three-dimensional soil-structure interaction problem. The soil's stress-strain behavior, including shear strength, stiffness and volume change characteristics and soil-pile interface, plays an important role in the response of piles subjected to lateral loads [1]. For that reason, in pile foundations the load-transfer mechanism is so complex and not fully understood yet [2].

In recent years, experimental model studies including the 1g model and centrifugal model tests were made on model short rigid piles in homogeneous soil conditions [3, 4, 5, 6, 7, 8, 9, 10, 11]. However, the majority of the existing design methods related to laterally loaded short rigid piles [12, 13, 14, 15, 16], except the methods proposed by Brinch Hansen [12] and Meyerhof et al. [14], are valid only for homogeneous soil conditions. There are numerous studies in the literature concerned with the application of the finite-element method for piles subjected to lateral loads [1, 2, 17, 18, 19, 20, 21, 22, 23, 24]. Most of the studies mentioned have been performed on long flexible piles in homogeneous soil conditions.

On the other hand, most of the soil deposits are a layered system and in reality piles are often embedded in layered soils. There are a few studies in the literature based on numerical analyses related to flexible piles subjected to lateral loads in layered soils [25, 26, 27]. Also, there is

limited information in the literature that attempted to explore the behavior of short rigid piles subjected to lateral loading in layered soil deposits and to investigate the factors affecting the lateral load capacity of short rigid piles in layered soils.

In this study, the behavior of a short rigid pile subjected to a lateral loading in a two-layer sand soil profile of different densities and thickness is investigated. For this purpose, a series of model test studies was carried out on model piles founded in homogeneous loose, homogeneous dense and two-layered sand conditions. The model tests were analyzed by a three-dimensional nonlinear finite-element method. Initially, in the numerical studies, a parametric study was performed in order to explore the effect of some parameters, such as the elasticity modulus, dilatancy and interface behavior of the sand on the lateral load capacity of short rigid piles. After the determination of the parametric values, model test studies were analyzed under the experimental ultimate lateral load capacities for each of the soil conditions considered to evaluate the failure regions developed around the pile and the distribution of the lateral effective stresses along the pile embedded depth under the experimental conditions. Finally, the lateral load capacities and the distributions of the lateral effective stresses were calculated using the methods proposed by Brinch Hansen [12] and Meyerhof et al. [14]. Then, the results obtained from these conventional methods were compared with the experimental and numerical results of this study.

2 EXPERIMENTAL TESTING PROGRAM

The loading tests were carried out in a steel box container. The internal dimensions of the test box were 960 × 480 mm in plan and 500 mm in height. The two side walls of the box were 10-mm-thick glass and the other sides and base plate were a 20-mm-thick wooden plate. The dimensions of the test box were chosen to be large enough to minimize the influence of the box boundaries. The inside walls of the test box were smooth and therefore the side friction effect was minimal. The distance between the pile tip and the base plate of the box was five times that of the pile diameter. A schematic view of the model test set-up is shown in Fig. 1.

a)

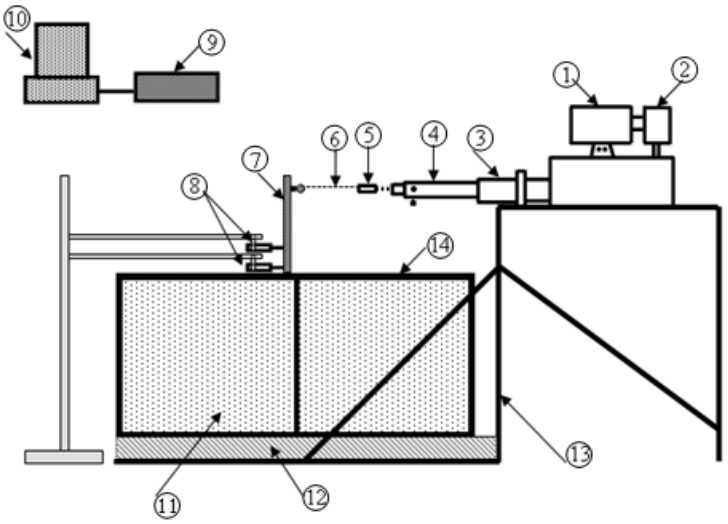

1. Motor
2. Reduction Gear
3. Loading Gear
4. Loading Tip
5. Load Cell
6. Steel Rope
7. Pulling Arm
8. Displacement Transducers
9. Data Logger
10. PC
11. Sand
12. Lifting Platform
13. Loading Table
14. Test Box

b)

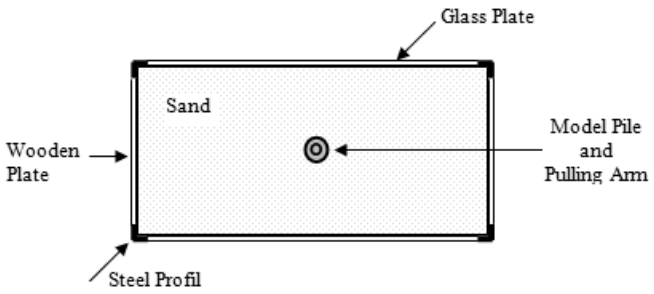

Figure 1. General layout of the apparatus for the model test: (a) side view (b) plan view.

The model tests were conducted on 1/20-scale model piles. A circular model pile with a diameter (D) of 50 mm and a length (L) of 200 mm was used in the tests. The model pile was fabricated from steel (E_{pile}=210000 MPa). The embedment ratio (L/D) of the pile was 4 in all the tests. A pulling arm, also fabricated from steel, with a diameter of 25 mm and a height of 330 mm was attached to the model pile, as seen in Fig. 2.

A short rigid pile can be described as one where the embedded length does not exceed ten times its lateral dimension [28]. On the other hand, Broms [13] showed that the embedment depth of a laterally loaded pile has to be less than $2T$ to behave as a rigid pile. In cohesionless soils, the value of the stiffness factor T is calculated as:

$$T = \sqrt[5]{\frac{E_{pile} I_{pile}}{n_h}} \qquad (1)$$

where:

$E_{pile}I_{pile}$; bending stiffness of the pile,
n_h ; coefficient of subgrade reaction.

The values of the coefficient of the subgrade reaction for the loose and dense conditions are 2200 and 17600 kN/m^3, respectively [29]. The estimated $2T$ values are 0.987 and 0.651 for the loose and dense sand conditions, respectively. The $2T$ values indicate that the model pile satisfies the criterion valid for a short rigid pile.

The lateral load was applied at a height of 300 mm as a pulling force. The lateral load was imposed at a constant rate of displacement of 1 mm/min. via a steel cable linked to a motorized pulling mechanism. The lateral displacement of the pulling arm was measured using two linear variable differential transducers (LVDTs) attached at the elevations of 26 mm and 86 mm above the sand's surface. The lateral load was monitored by a 1-kN capacity load cell. The output from the load cell and transducers was fed to an ADU data logger. The data was converted using DIALOG software to produce the values of the lateral displacement and lateral load. The lateral load was applied until 10 mm of deflection occurred at the point that was 86 mm above the sand's surface.

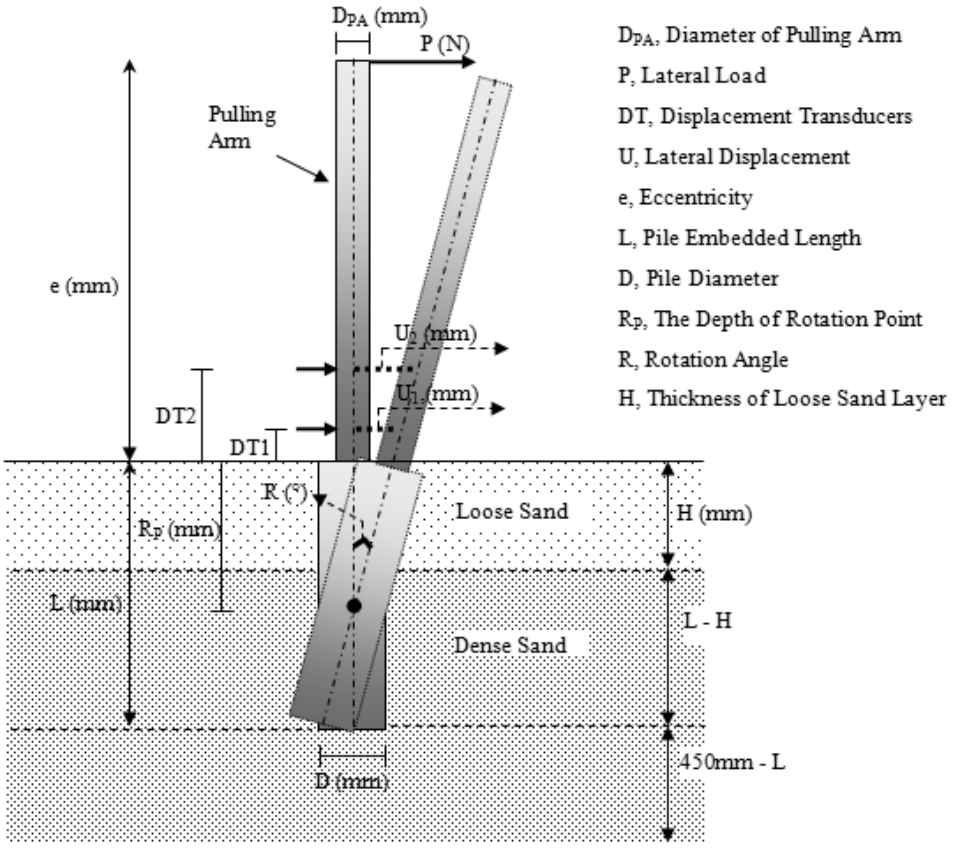

Figure 2. The geometry of the model system.

3 SOIL DESCRIPTION AND PREPARATION OF THE SAND BED

The model tests were performed in dry sand obtained from the Cakit river bed. The sand used in the tests was classified as poorly graded sand (*SP*). The effective grain size (D_{10}), uniformity coefficient (U_c) and the coefficient of curvature (U'_c) of the sand were 0.18 mm, 2.78 and 1.00, respectively. The model sand was prepared in the homogeneous loose, homogenous dense and layered sand conditions. The dry unit weights (γ_{dry}) of the sand were 15.03 kN/m^3 and 17.06 kN/m^3 for the loose and dense sand conditions, respectively. The internal friction angles (ϕ') obtained from triaxial compression tests were 38° and 44° for the loose and dense sand packings, respectively.

The sand was placed into the test box in layers of 30 mm thickness in both the loose and dense sand conditions. The required sand weights were calculated for each layer at the beginning of the experiment. For the loose state, the sand was poured into the test box from a height that is as close as possible and then the sand was spread out in the test box, utilizing the scale lines on the glass plates of the test box. For the dense state, in addition to the processes performed in the loose condition, each layer was compacted using a hand-held vibratory compactor. After the compaction, the thickness of the layer was controlled using the scale lines on the glass plates. When the preparation of the sand bed was completed up to the level of the pile tip, the model pile was placed at the centre of the test box, guided by an apparatus to assure centric vertical alignment. In this way the movement of the pile was also prevented. After securing the pile in place, sand was placed up to the top level of the pile.

4 TEST RESULTS

The ultimate lateral load capacity from lateral pile load tests is determined depending on the structure supported by the piles [30]. In the literature, different assumptions concerning with the ultimate lateral load capacity have been used by different researchers. The assumptions made by researchers were generally based on the excessive lateral displacement of the pile head or the rotation of the pile [10]. On the other hand, some researchers defined the lateral load capacity of the pile from the load-displacement or moment-rotation curves as the point where the curve becomes linear or substantially linear [7, 8, 15]. Sawwaf [31] performed a series of laboratory model tests on rigid model piles to investigate the effect of reinforcing on the earth slope on the lateral behavior of a single vertical pile located near the slope. Sawwaf [31] defined the pile lateral capacities as the loads corresponding to the points wherein the lateral displacements of the pile equal to 10 and 20% of the pile diameter evaluating the effect of different parameters. In the present study, the lateral load corresponding to the lateral displacement equal to 10% of the pile diameter at the pile head was defined as the ultimate lateral load capacity.

In the experimental studies, five lateral loading tests were carried out to investigate the lateral behavior of a short rigid pile founded in layered sand deposits. The layered sand profile consisted of a loose sand layer overlying a dense sand layer, as encountered in most cases. The layer thicknesses were described using the *H/L* ratio. As shown in Fig. 2., *H* is the thickness of the loose sand layer and *L* is the embedded depth of the pile. The tests were performed for the ratio of *H/L*=0.25, 0.50, 0.75 and also for the homogenous loose (*HL*) and homogeneous dense (*HD*) sand conditions.

The experimental lateral load-lateral displacement relations at the pile head are presented in Fig. 3. The ultimate lateral load capacities ($P_{ultimate}$), the depths of the rotation point (R_D) and the rotation degrees (R) at the pile head for $u_{x=0}$=5mm obtained from experiments for the homogeneous and layered sand conditions are summarized in Table 1. As seen in Table 1, the lateral load capacities obtained in the layered conditions decrease as the thickness of the upper loose sand layer increases. In addition, in the layered sand conditions, the depth of the rotation point (zero horizontal displacement point) moves towards the pile tip with an increasing thickness of the upper loose sand layer.

Table 1. Model test results.

	HD = *H/L*=0	*H/L* = 0.25	*H/L* = 0.50	*H/L* = 0.75	*HL*=*H/L*=1
$u_{x=0}$ (mm)	5	5	5	5	5
$P_{ultimate}$ (N)	56.641	46.249	24.576	16.149	10.299
R_D (%)	75.019	75.346	80.421	84.971	76.475
R (°)	1.893	1.888	1.766	1.670	1.854

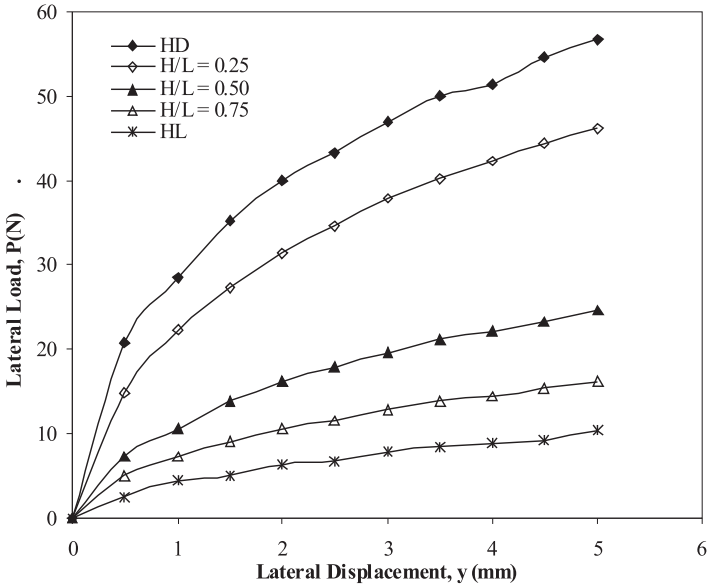

Figure 3. Experimental lateral load-lateral displacement relationships at the pile head.

As shown in Fig. 3., the experimental relations are non-linear and become softer with the increasing thickness of the loose sand layer. There is no observed peak strength in the experimental results shown in this figure. The lateral load capacity of the pile in the case of H/L=0.25 is 19% lower than the lateral load capacity obtained in the case of homogeneous dense sand. This ratio is 57% and 71% for the cases of H/L=0.50 and H/L=0.75, respectively. It is clear that the soil packing markedly effects the lateral load capacity of short rigid piles. The lateral load capacity of the pile in homogeneous dense sand is approximately five times that in homogeneous loose sand.

The ultimate lateral load capacity of short rigid pile is essentially provided by the mobilization of passive resistance in the soil; in other words, it is significantly dependent on ϕ'. The values of the lateral passive pressures acting on opposite faces above and below the rotation point will decrease as the thickness of the upper loose sand layer increases. The decrease in the lateral resistance is mainly due to the lower stiffness of the upper loose sand layer. In addition, the smaller unit weight of the loose sand results in smaller effective stresses in the dense sand layer compared with the condition of the homogeneous dense sand. On the other hand, in the layered sand condition, the presence of the dense sand layer caused the layered system to be stiffer than the homogeneous loose sand and increased the lateral load capacity significantly with respect to the case of the homogeneous loose sand. The reduction in the lateral load capacity with respect to the value obtained in the case of the homogeneous dense sand is not directly proportional to the layer thicknesses.

If the $P_{ultimate}$ values are normalized using the weight of the pile (W_{pile}), a non-dimensional relationship between $P_{ultimate}/W_{pile}$ and H/L for values of H/L in the range 0~1 can be obtained. The relationship illustrated in Fig. 4. may be given by the following equation. The R^2 value of the equation was found to be 0.98.

$$P_{ultimate} = 1.45\ e^{-1.79\,(H/L)}\ W_{pile} \qquad (2)$$

Equation 2 was obtained as an approximation of the model test results performed in the experimental studies. This equation can be used only in the conditions valid in the model tests performed. This equation is not applicable for different soil conditions.

5 FINITE-ELEMENT ANALYSES

Finite-element (FE) studies of model tests of short rigid piles subjected to lateral loading with the same geometries and same soil conditions as in the model tests were carried out using the three-dimensional (3D) non-linear computer program PLAXIS 3D Foundation. The program is formulated using the displacement method and uses constitutive models based on plasticity theory.

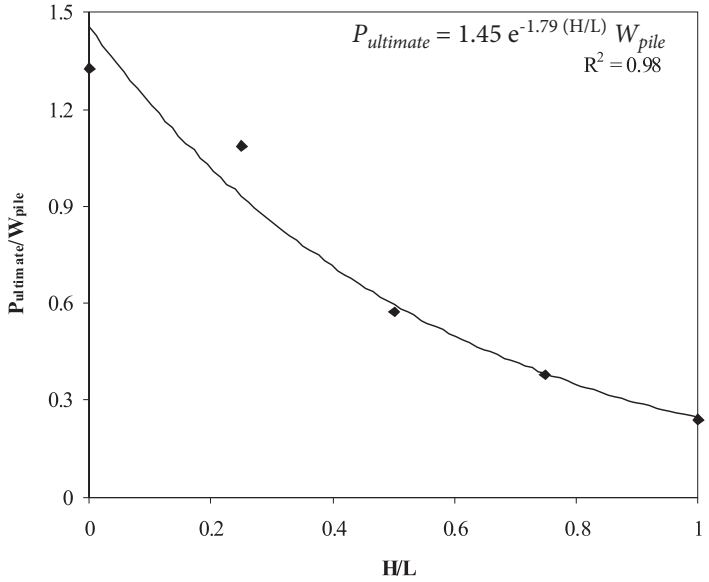

Figure 4. The non-dimensional relationship between the ultimate lateral load capacity and *H/L*.

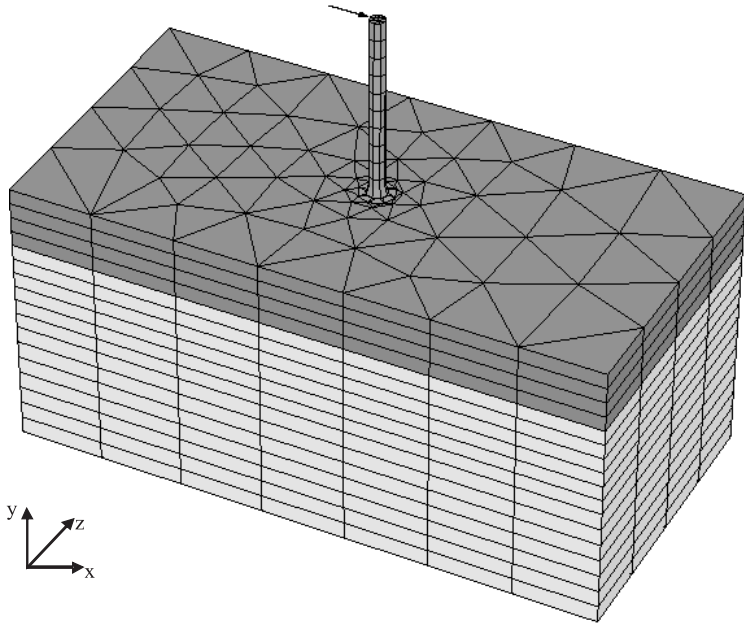

Figure 5. Three-dimensional finite-element mesh for layered sand condition.

The mesh density including the number of nodes, the number of elements and the average element size were defined after performing a series of trial analyses with several meshes of increasing refinement. The analyses were carried out until no significant changes were observed with further refinement. The medium-fine mesh density, which means the horizontal and vertical element distributions, respectively, was selected at the end of the analyses. The selected mesh density is also refined using the additional horizontal planes called work planes in the vertical direction along the pile length in order to provide greater accuracy in the results. PLAXIS 3D Foundation refines the mesh automatically in the area surrounding the pile. Therefore, the size of the elements located around the pile was smaller. A typical mesh for 3D FE analyses in the case of the layered sand condition

is shown in Fig. 5. PLAXIS 3D Foundation incorporates a fully automatic mesh-generation procedure to create the 3D FE mesh. The 3D mesh was generated in two stages. Firstly, a two-dimensional (2D) mesh consisting of six-noded triangular elements was automatically created. Then, the 2D mesh was refined around the pile. In the second stage, this 2D mesh was extended into a 3D mesh compounded of 15-noded wedge elements. The 15-noded wedge element is composed of 6-noded triangles in the horizontal direction and 8-noded quadrilaterals in the vertical direction. In this type of 3D elements, three nodes are located along each edge, which provide a quadratic approximation of the displacement field within the volume of the element [32].

The pile is modeled as a solid pile using volume elements in the centre of the mesh. To model the interaction between the sand and pile an interface was created along the entire circumference of the pile. The sand-pile interface is modeled by means of interface elements. Sixteen-noded interface elements with zero thickness were used to simulate the soil-pile interaction. The interface elements can be smooth or fully rough. The properties of the interface are defined by the interface-strength-reduction factor (R_{inter}). The value of the R_{inter} factor was defined for each of the soil conditions by calibrating the analyses results with respect to the tests results. In the analyses, the installation effects of the pile are not taken into account. An elastic-plastic model is used to define the behavior of the interface elements. The relationship between the normal pressure and the shear force is governed by the Coulomb criterion. The interface elements allow the development of slipping behavior between the sand and the pile.

It was assumed that the lateral load is acting at a height of 6 m above the sand surface as a lateral point load in prototype dimensions since this is the approximate height of most laterally loaded structures. In the analyses, the lateral load was imposed directly to the top level of the pulling arm as a point load. The pulling arm is also modeled as a solid pile using the volume elements.

All the nodes on the model's vertical boundaries, i.e., the nodes on the end of the *x-y* and *y-z* planes, were restrained in the x and z directions, respectively. All the nodes on the model bottom boundary were fixed in all three directions (*x*, *y* and *z*).

The pile and pulling arm were assumed to be linearly elastic. The Mohr-Coulomb (MC) material model was used to simulate the non-linear sand behavior because of its simplicity, reasonable number of model parameters and reasonable accuracy in modeling the behavior of the laterally loaded pile problem. The MC model has a fixed yield surface and the yield surface is not affected by plastic straining. For MC-type yield functions, the theory of associated plasticity overestimates the dilatancy. Therefore, in addition to the yield function, a plastic potential function is introduced. The plastic potential function contains the parameter of dilatancy angle that is required to model positive plastic volumetric strain increments. The elastic-plastic MC model involves five basic input parameters: elasticity modulus (E), Poisson's ratio (ν), internal friction angle (ϕ'), cohesion (c') and dilatancy angle (ψ).

The friction angles of the sand were 38° and 44°, based on the drained triaxial compression test results for the loose and dense sand packings, respectively. Direct shear tests on the sand samples were also conducted to determine the angles of internal friction. Accordingly, ϕ' values of 39.27° and 45.67° were obtained at dry unit weights of 15.03 kN/m^3 and 17.06 kN/m^3, corresponding to the loose and dense sand packings, respectively. The value of the secant elastic modulus (E_{50}) of the sand, in both loose and dense sand conditions, was obtained from the drained triaxial compression tests. The values of E_{50} were 20600 kPa and 30000 kPa for the loose and dense sand conditions, respectively. The dilatancy angle of the sand was evaluated according to the equations proposed by Bolton [33] and PLAXIS for quartz sand. The values of Poisson's ratio generally lay between 0.20 and 0.40 in the sand; therefore, an average value of 0.30 was used in the computations [34]. To avoid complications in the analyses performed in dry cohesionless soils (c'=0), PLAXIS offers to enter a small value that is bigger than 0.20 kPa for c'. For that reason, a value of 0.30 kPa was used for the c' in the analyses.

The initial stresses in the numerical modeling were generated using Jaky's formula, which gives the at rest earth pressure coefficient K_0 =1-sinϕ'[35]. In order to obtain load-displacement relationships at the pile head the total lateral load is applied in stages.

6 PARAMETRIC STUDIES

In this section, parametric studies were conducted, both in loose and dense sand conditions, to investigate the influences of the elasticity modulus of sand, the sand dilatancy and the interface strength on the response of a short rigid pile subjected to a lateral load using the non-linear finite-element approach. The effects of these parameters can not easily be evaluated experimentally in the model loading tests.

The model calibration was made by comparing the results of the FE analyses with those from model tests

to determine the optimum values of the parameters. Thus, numerical models, for both loose and dense sand conditions, which produce the most reliable results with respect to the test results, were obtained. The value of the applied lateral load in the parametric analyses carried out in homogeneous loose sand was 40 N, while it was 80 N in homogeneous dense sand.

The effect of the elasticity modulus of the sand on the lateral response of the model pile is considered herein by keeping the values of the sand dilatancy and interface strength constant and changing the values of the elasticity modulus. The same procedure was applied while investigating the effects of other two parameters, i.e., the sand dilatancy and the interface strength.

6.1 ELASTICITY MODULUS

The strength and stiffness of the sand are generally assumed as increasing with depth. The sands exhibit non-linear and irreversible deformation behavior under loading. The deformability or stiffness of the sand varies depending on the void ratio extent, which means the difference between the maximum and minimum void ratios. On the other hand, the elasticity modulus of sand increases with effective confining stress and the elasticity modulus is not proportional to the effective confining stress [36]. It is reasonable to assume that the elasticity modulus increasing linearly with depth for sands and acceptable solutions can be obtained in this way [26, 37]. In contrast, the modulus of elasticity of sand is constant in the horizontal direction [29]. In many cases encountered in practice, the elasticity modulus of sand would not increase linearly with depth.

In PLAXIS 3D Foundation, the value of the elasticity modulus is normally constant through the depth when using the MC material model to simulate the stress-strain behavior of sand. The reference elasticity modulus ($E_{reference}$) is the value of the elasticity modulus of sand determined at the level of the reference depth ($y_{reference}$). In the homogeneous loose and dense sand conditions, the $y_{reference}$ is equal to zero and $E_{reference}$ is determined at the level of the sand surface. However, the increment of elasticity modulus with depth can be considered using the $E_{increment}$ option. This option defines the amount of increment per unit of depth.

The influence of the elasticity modulus of sand on the lateral response of a short rigid pile subjected to lateral loading was investigated, assuming that the elasticity modulus was a function that is linearly dependent on the depth of the sand layer. The values of the constant parameters a (slope) and b (intercept) of the linear relationship $y = a + bx$ were derived as an example for the homogeneous loose sand condition. The value of the secant elasticity modulus (E_{50}) of loose sand defined considering the stress-strain curve obtained from drained triaxial compression test conducted under the confining pressure equal to 100 kPa was 20600 kPa. The dry unit weight of the loose sand was 15.03 kN/m^3. An effective stress value

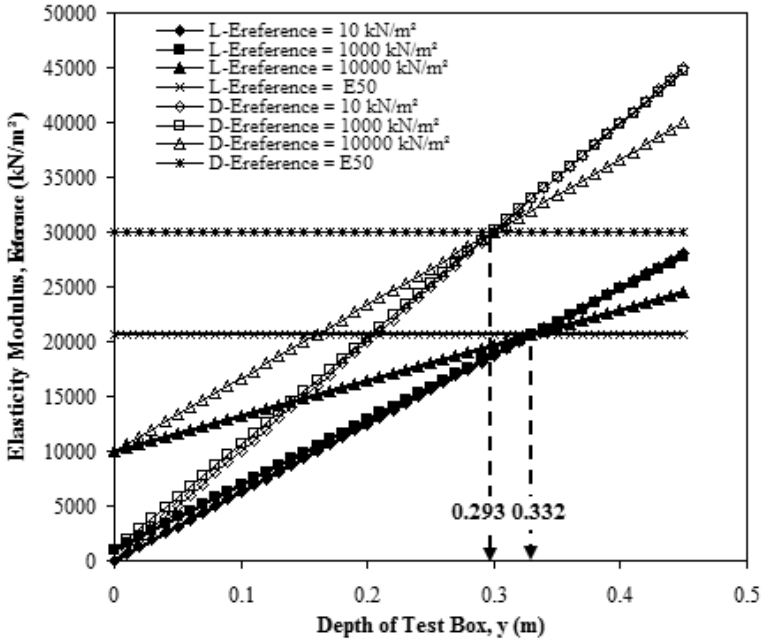

Figure 6. Elasticity modulus functions in the loose (L) and dense (D) sand conditions.

of 100 kPa can be obtained at a depth of 6.65 m below the sand surface in the homogeneous loose sand layer in the prototype conditions. However, this prototype depth corresponds to a depth of 33 cm in the model dimensions. If we assume that the value of elasticity modulus increases linearly with depth, the value of $E_{reference}$ determined at the level of the sand surface will increase as well as $E_{increment}$ per unit depth and it will be equal to E_{50} at the depth of 33 cm. The function defining the variation of the elasticity modulus with depth is described as follows:

$$E = E_{reference} + E_{increment}\, y \qquad (3)$$

where y represents the depth in the sand layer.

Fig. 6 shows the elasticity modulus functions obtained in loose and dense sands for different values of $E_{reference}$. In order to study the effect of the elasticity modulus in loose and dense sand conditions, a series of analyses were carried out for four different values of $E_{reference}$ chosen at the beginning of the analyses. The results of the numerical analyses are summarized in Tables 2 and 3 for the loose and dense sand conditions, respectively. Figs. 7 and 8 illustrate the lateral load-lateral displacement relations observed at the pile head for the loose and dense conditions, respectively.

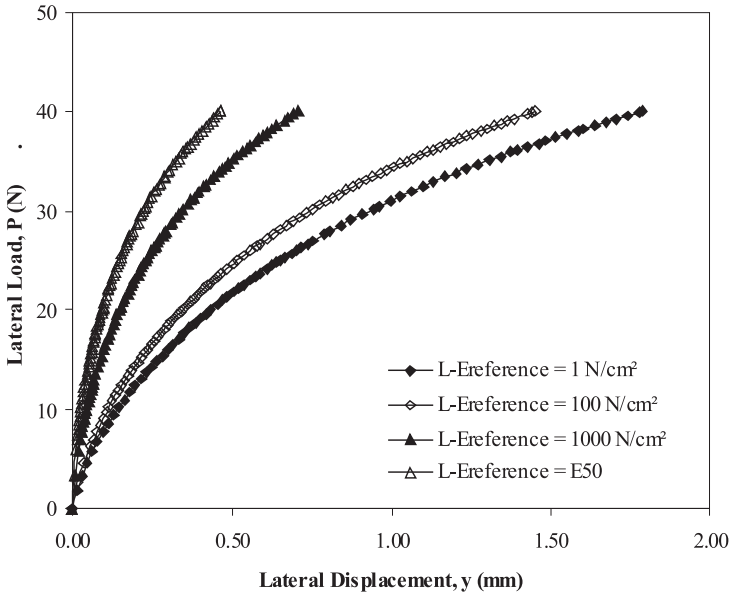

Figure 7. The effect of elasticity modulus of sand in the loose (*L*) sand condition.

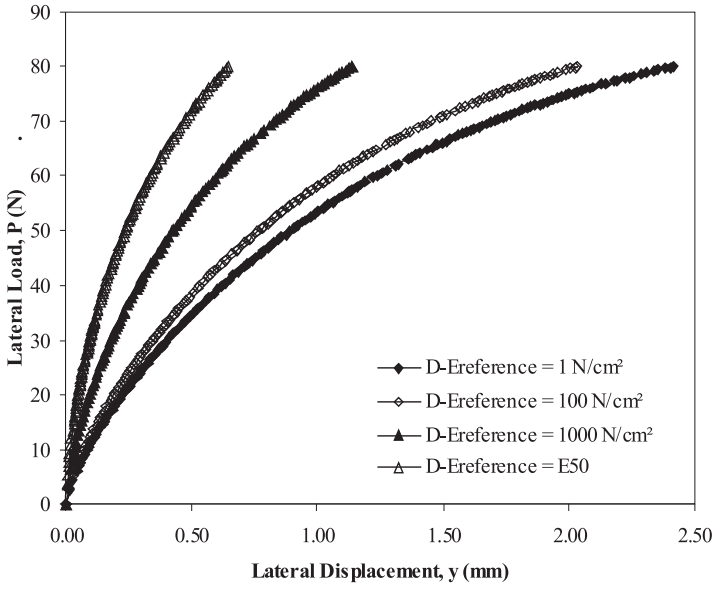

Figure 8. The effect of elasticity modulus of sand in the dense (*D*) sand condition.

Table 2. The effect of the elasticity modulus in loose sand.

$E_{reference}$ (N/cm^2)	1	100	1000	E_{50} = 2060
$E_{increment}$ (N/cm^2/cm)	62.400	59.400	32.121	0
ψ (°)	8	8	8	8
R_{inter}	0.700	0.700	0.700	0.700
P (N)	40	40	40	40
$u_{x=0}$ (cm)	0.178	0.145	0.070	0.046
R_D (%)	73	72	66	62
R (°)	0.695	0.572	0.301	0.210

Table 3. The effect of the elasticity modulus in dense sand.

$E_{reference}$ (N/cm^2)	1	100	1000	E_{50} = 3000
$E_{increment}$ (N/cm^2/cm)	102	98.970	68.250	0
ψ (°)	14	14	14	14
R_{inter}	0.700	0.700	0.700	0.700
P (N)	80	80	80	80
$u_{x=0}$ (cm)	0.241	0.203	0.113	0.064
R_D (%)	70	69	64	59
R (°)	0.987	0.838	0.498	0.309

Similar behaviors were observed against the variation of the value of $E_{reference}$ in both loose and dense sand conditions.

As seen in Tables 2 and 3, as expected, the lateral displacements observed at the pile head decrease with an increasing value of $E_{reference}$. In addition, the depths of the rotation point move towards the sand surface. The value of the lateral displacement at the pile head in the case of $E_{reference}$=E_{50} is approximately 74% smaller than that obtained in the case of $E_{reference}$=1 N/cm^2. However, the lateral load capacity in the case of $E_{reference}$=1 N/cm^2 is nearly 48% smaller than that of the case of $E_{reference}$=E_{50} for the same lateral displacement in both loose and dense sand conditions. As shown in Figs. 7 and 8, the relations are non-linear for both loose and dense sand conditions. As seen in Figs. 7 and 8, the load-displacement behaviors are stiffer and provide a higher lateral load capacity with the increasing value of $E_{reference}$ for the same lateral displacement value in both loose and dense sand conditions.

In layered sand conditions, the depth to obtain an effective stress value equal to 100 kPa, considering the layer structure, was calculated using a similar procedure as in the homogeneous sand conditions. Then, the values of the $E_{reference}$ and $E_{increment}$ at the beginning of the dense sand layer were defined using the values of $E_{reference}$ and $E_{increment}$ chosen for the upper loose sand layer with respect to the results of the parametric analyses.

6.2 SAND DILATANCY

The internal friction angle (ϕ') is the principal parameter when predicting the behavior of laterally loaded piles embedded in sand using theoretical methods. However, these methods [12, 13, 14, 15] ignore the effect of the volume change characteristics of sands based on the dilatancy of the pile's response. However, the effect of the dilatancy of the sands on the lateral response of piles subjected to lateral loading cannot also be investigated experimentally by model test studies. Therefore, the role that sand dilatancy plays in the lateral load capacity of the pile remains unknown [1].

In order to investigate the effect of dilatancy on the behavior of laterally loaded short rigid piles founded in sand a series of non-linear FE analyses were carried out. In the analyses, two different approaches suggested by Bolton [33] and PLAXIS associated with the value of critical internal friction angle ($\phi'_{critical}$) of quartz sand were used to calculate the dilatancy angle of the sand. The values of the dilatancy angle were obtained using the following formula:

$$\phi' = \phi'_{critical} + \psi \qquad (4)$$

The value of $\phi'_{critical}$ for quartz sand has been proposed as 33° by Bolton [33], while PLAXIS suggests this value

Table 4. The effect of the dilatancy angle in loose sand.

$E_{reference}$ (N/cm^2)	1	1
$E_{increment}$ (N/cm^2/cm)	62.400	62.400
ψ (°)	5	8
R_{inter}	0.700	0.700
P (N)	40	40
$u_{x=0}$ (cm)	0.207	0.178
R_D (%)	73	73
R (°)	0.807	0.695

Table 5. The effect of the dilatancy angle in dense sand.

$E_{reference}$ (N/cm^2)	1	1
$E_{increment}$ (N/cm^2/cm)	102	102
ψ (°)	11	14
R_{inter}	0.700	0.700
P (N)	80	80
$u_{x=0}$ (cm)	0.284	0.241
R_D (%)	70	70
R (°)	1.168	0.987

should be 30°. The internal friction angles were 38° and 44° for the loose and dense sand conditions, respectively, in the analyses. The analyses were conducted in both loose and dense sand conditions. The results of the analyses are presented in Tables 4 and 5 for the loose and dense sand conditions, respectively. The plots of the lateral load-lateral displacement relations at the pile head for different dilatancy angles are shown in Figs. 9 and 10 for the loose and dense sand conditions, respectively.

As seen in Tables 4 and 5, for both loose and dense sand conditions, the lateral displacement observed at the pile head decreases by nearly 15% with the increasing value of dilatancy angle. However, the depth of the rotation point is not affected by the variation of the dilatancy angle. Thus, it can be concluded that the volume of the sand mass mobilized under the lateral load will be more in the case of higher dilatation values. As a result, the higher dilatation values will provide greater lateral load capacities.

As shown in Figs. 9 and 10, for both loose and dense sand conditions, the effect of sand dilatancy on the lateral load capacity is seen more clearly with an increasing lateral displacement at the pile head. At first, especially for the small values of the lateral displacement, the effect of dilatancy is not distinct and the curves obtained for different dilatancy angles are overlapped. The sand mass compressed under the lateral loading becomes denser as the lateral displacement increases. As a result, the effect of the dilatancy property in sands arises as an extra contribution to their strengths.

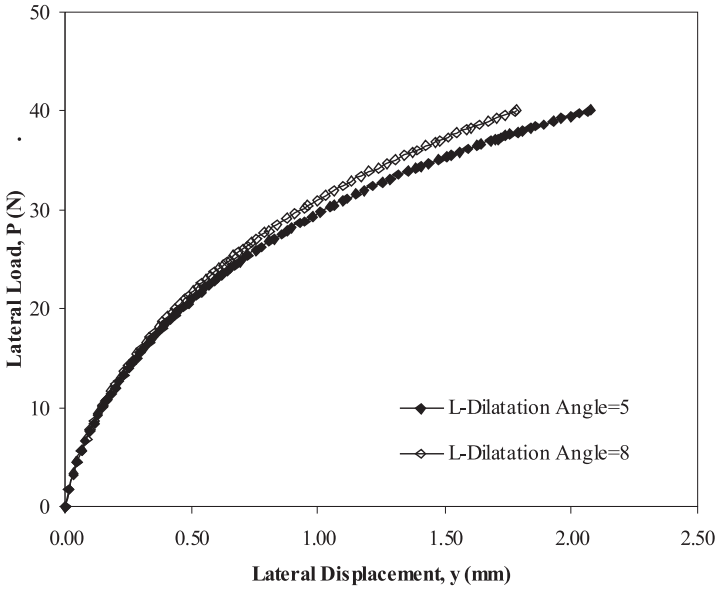

Figure 9. The effect of sand dilatancy in the loose (*L*) sand condition.

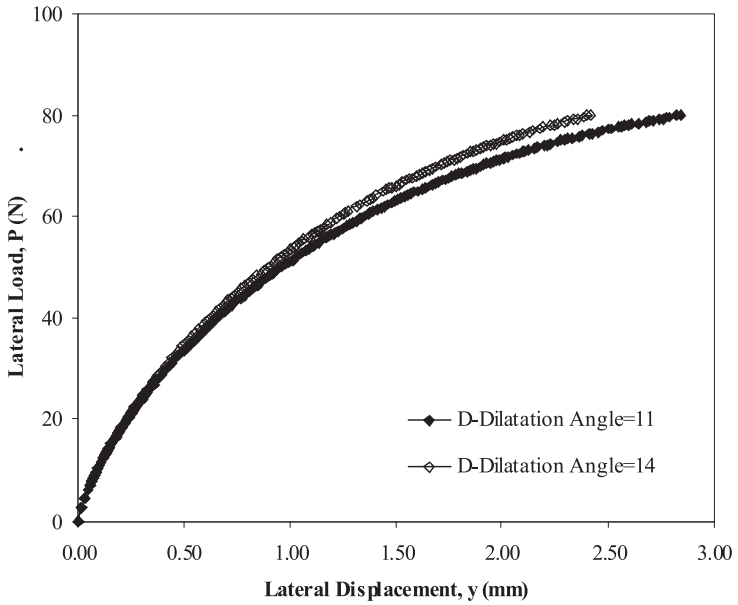

Figure 10. The effect of sand dilatancy in the dense (*D*) sand condition.

6.3 INTERFACE BEHAVIOR

The soil-structure interaction has a significant effect on the performance of buried structures. The correct modeling of the load-transfer characteristics of the soil-structure interface is very important in predicting the behavior of buried structures using numerical methods [38].

The main parameter represented the interface behavior is the strength-reduction factor (R_{inter}). The side friction between the pile and the soil is modeled by choosing a suitable value for R_{inter}. R_{inter} relates the interface strength to the soil strength. The interface properties are calculated from the soil properties in the associated data set and R_{inter} by applying the following rules;

$$c_i = R_{inter}\, c_{soil} \qquad (5)$$

$$\tan\phi_i = R_{inter} \tan\phi_{soil} \le \phi \tan\phi_{soil} \qquad (6)$$

$$\psi_i = 0° \text{ for } R_{inter} < 1, \text{ otherwise } \psi_i = \psi_{soil} \qquad (7)$$

In general, for a real soil-structure interaction, the interface is weaker and more flexible than the associated soil layer, which means that the value of R_{inter} should be less than 1. PLAXIS, generally, assumes that the interface properties are equal to two-thirds of the soil properties (i.e. R_{inter}=0.67).

Some factors, such as the installation method of the pile, the relative density of the sand, the roughness of the pile surface and pile material, would affect the behavior of the interface element. Therefore, the value of R_{inter} should be decided after considering these factors. On the other hand, the installation method of the pile cannot be taken into account in PLAXIS. In addition, the model pile used in the model test studies was a buried pile and the surface of the pile was smooth in all the tests. Further, when the grain size of the sand used in the model tests was considered, the value of 0.67 for R_{inter} may be unrealistic when analyzing the model tests. Hence, the value of R_{inter} was determined by a trial-and-error approach in the analyses performed in both loose and dense conditions by comparing the load-displacement relations obtained from numerical analyses and model tests.

The interface elements can transmit only shear forces along their surfaces when they are subjected to a compressive normal pressure. When the shear stress reaches the bond strength, governed by the Coulomb criterion, a large relative displacement (slip) occurs [38]. The distinction between the elastic behavior, where small displacements can occur within the interface, and plastic interface behavior, when permanent slip may occur, is made using the Coulomb criterion. For the elastic behavior of the interface, the shear stress τ is given by:

$$|t| < s_n \tan f_i + c_i \qquad (8)$$

$$|t| = \sqrt{t_{s1}^{\,2} + t_{s2}^{\,2}} \qquad (9)$$

where:

τ_{s1} and τ_{s2}; shear stresses in the two (perpendicular) shear directions,

σ_n; effective normal stress.

For plastic behavior τ is evaluated using the following formula:

$$|t| = s_n \tan f_i + c_i \qquad (10)$$

where:

ϕ_i and c_i; the friction angle and cohesion of the interface, respectively.

The numerical results are summarized in Table 6 and Table 7 for the loose and dense sand conditions, respectively. The results of the analyses are also presented in terms of lateral load-displacement relationships at the pile head in graphical form in Figs. 11 and 12 for the loose and dense sand conditions, respectively.

Similar behaviors were obtained in both loose and dense sand conditions. As seen in Tables 6 and 7, the lateral displacement at the pile head decreases with the increasing value of the R_{inter}. However, the depth of the rotation point moves towards the sand surface as the value of R_{inter} increases.

As shown in Figs. 11 and 12, R_{inter} has a significant effect on the lateral load capacity of the short rigid pile for both loose and dense sand conditions. Such that, the lateral load capacity of the short rigid pile in loose sand in the case of R_{inter}=0.03 is equal to 16% of the lateral load capacity obtained in the case of R_{inter}=0.70 for the same lateral displacement. Similarly, in the dense sand condition, the lateral load capacity value obtained in

Table 6. The effect of the interface behaviour in loose sand.

$E_{reference}$ (N/cm^2)	1	1	1
$E_{increment}$ (N/cm^2/cm)	62.400	62.400	62.400
ψ (°)	5	5	5
R_{inter}	0.030	0.350	0.700
P (N)	40	40	40
$u_{x=0}$ (cm)	5.425	0.292	0.207
R_D (%)	90	75	73
R (°)	16.690	3.285	0.807

Table 7. The effect of the interface behaviour in dense sand.

$E_{reference}$ (N/cm^2)	1	1	1
$E_{increment}$ (N/cm^2/cm)	102	102	102
ψ (°)	11	11	11
R_{inter}	0.130	0.350	0.700
P (N)	80	80	80
$u_{x=0}$ (cm)	0.585	0.417	0.284
R_D (%)	81	73	69
R (°)	2.054	1.634	1.168

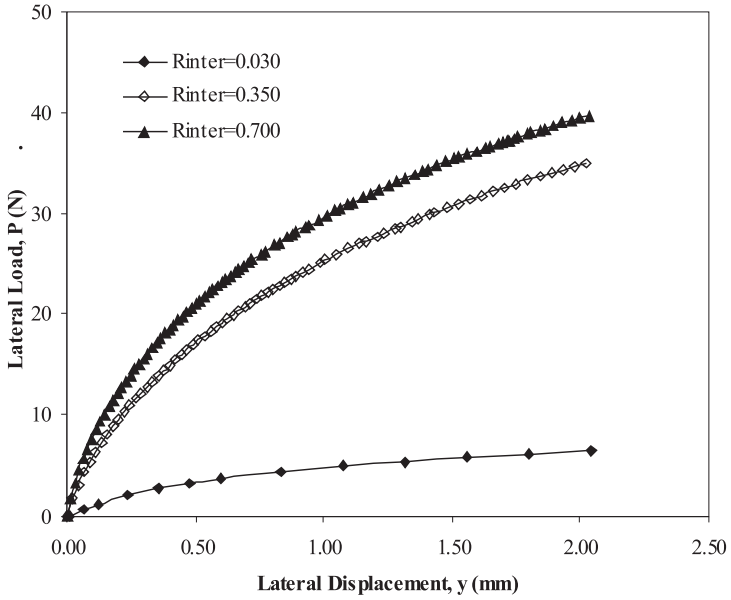

Figure 11. The effect of the interface behavior in the loose (*L*) sand condition.

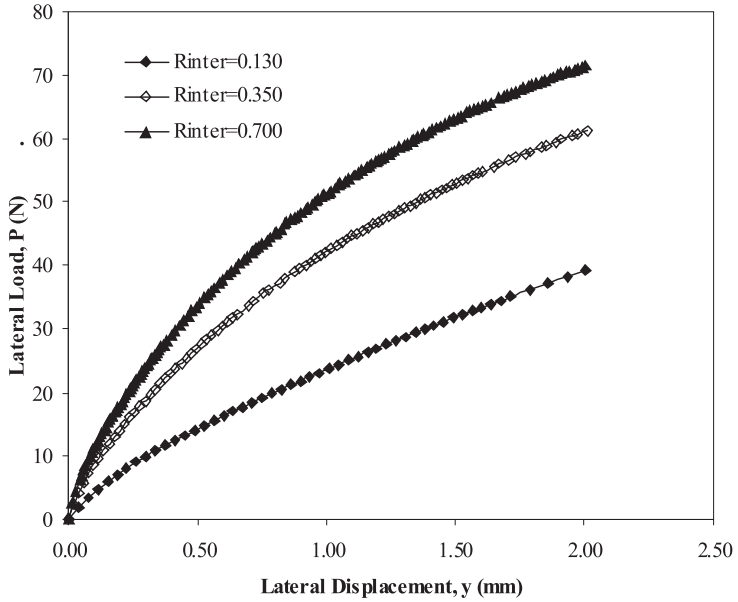

Figure 12. The effect of the interface behavior in the dense (*D*) sand condition.

the case of R_{inter}=0.13 is as well as the 54% of the value obtained in the case of R_{inter}=0.70 for the same lateral displacement. The load-displacement curves exhibit stiffer behavior depending on the increasing value of R_{inter}.

Fig. 13 indicates the effect of R_{inter} on the interaction between the sand and the pile. As shown in Fig. 13, the degree of permanent slipping behavior between the pile and the sand surfaces decreases depending on the decreasing value of R_{inter}. As a result, the frictional behavior between the surfaces decreases. Since the interface elements can not transfer shear forces across their surfaces completely when they are subjected to a compressive normal pressure, the lateral load capacity of the pile will decrease.

On the other hand, the values of $\tan\phi_i$ and c_i are calculated by multiplying the R_{inter} value with the soil properties, as shown in eqs. 5 and 6. Therefore, even if the normal soil resistance in front of the pile is unchanged, the slipping behavior along the interface will occur at different shear strength values, depending on the chosen R_{inter} value and the criteria used in modeling the interface behavior.

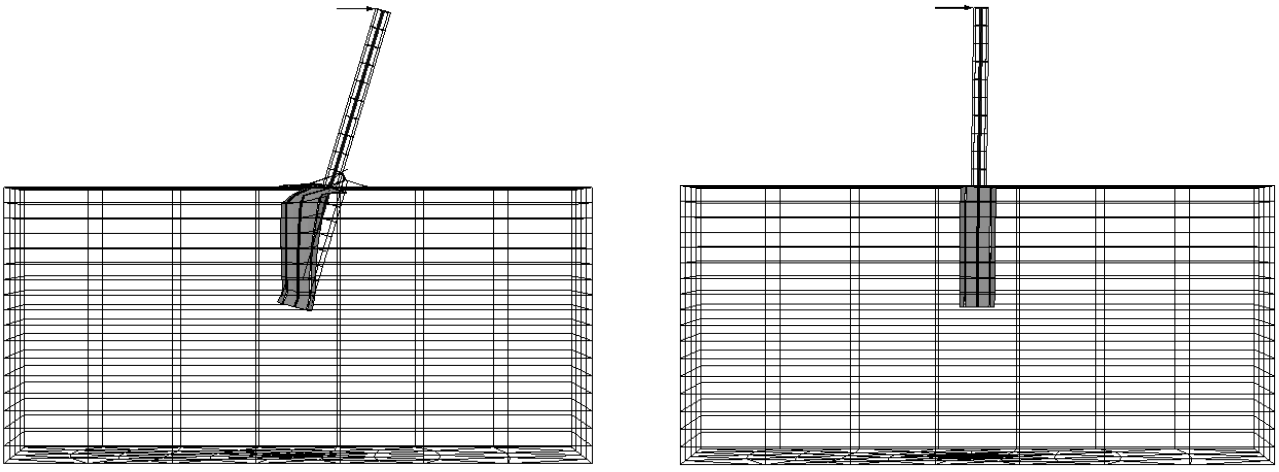

R_{inter} = 0.030 R_{inter} = 0.700

Figure 13. The effect of the R_{inter} on the interaction between the sand and the pile.

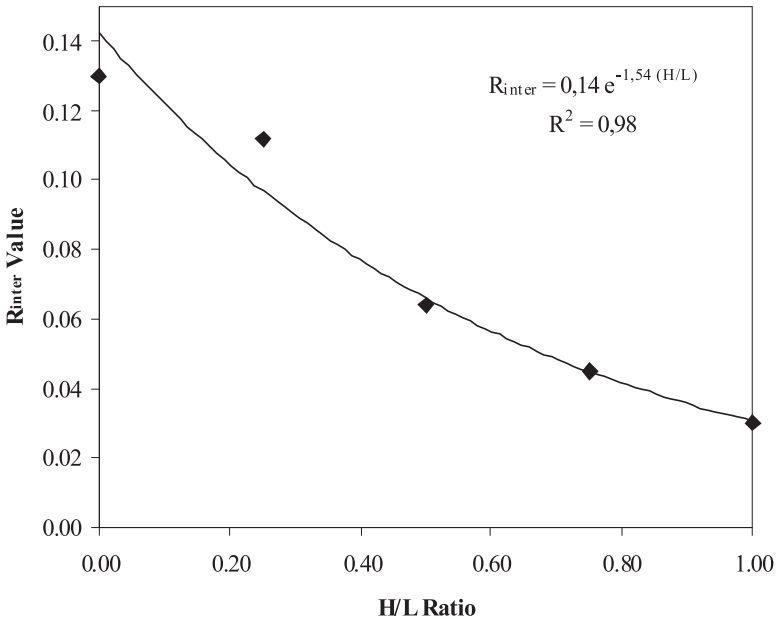

Figure 14. The variation of the R_{inter} with the H/L ratio.

The interface behavior is significantly dependent on the sand's density. Therefore, it is not reliable to use the values of R_{inter} obtained for the homogeneous loose and dense sand in the layered sand conditions having different layer thicknesses. It is necessary to define the average value of R_{inter} that is valid through the layered sand profile for each of the layered structure. A series of analyses were performed in the layered sand conditions in order to define the R_{inter} values that belong to each layer of the structure. The lateral load-displacement curves obtained from numerical analyses were compared with the curves obtained from model tests to calibrate the values of R_{inter}. The relationship obtained between R_{inter} and H/L is shown in Fig.14. The relation between R_{inter} and H/L was fitted with the following equation:

$$R_{inter} = 0.14\ e^{-1.54\,(H/L)} \qquad (11)$$

The R^2 value of the equation was obtained as 98%. Equation 11 has been obtained as an approximation of the results of the experimental studies and numerical analyses. This equation can only be used in the conditions valid in the model tests performed. This equation is not applicable for different soil conditions.

7 RESULTS AND DISCUSSION

At the end of the parametric studies, the values of the parameters that produced the most reliable results with respect to the model test results were obtained. The

Table 8. The selected values of parameters obtained from the finite-element analyses.

		HD=*H*/*L*=0	*H*/*L* = 0.25	*H*/*L* = 0.50	*H*/*L* = 0.75	*HL*=*H*/*L*=1
$E_{reference}$ (N/cm^2)	Loose	1	1	1	1	1
	Dense		313	625	937	
$E_{increment}$ (N/cm^2/cm)	Loose	102	62.40	62.40	62.40	62.400
	Dense		108	118.75	129	
$y_{reference}$ (cm)	Loose	0	0	0	0	0
	Dense		-5	-10	-15	
ψ (°)	Loose	11	5	5	5	5
	Dense		11	11	11	
R_{inter}		0.130	0.112	0.064	0.045	0.030

* HD means the homogeneous dense sand[1]
** HL means the homogeneous loose sand[2]

values of the parameters chosen at the end of the parametric analyses are listed in Table 8.

After the determination of the values of the parameters, finite-element models were analyzed under lateral loads equal to he ultimate lateral load capacities obtained in the model tests for each of the soil conditions. Thus, as the distribution of the lateral effective stresses along the pile embedded depth, the failure regions occurred around the model pile and the deformation behavior of

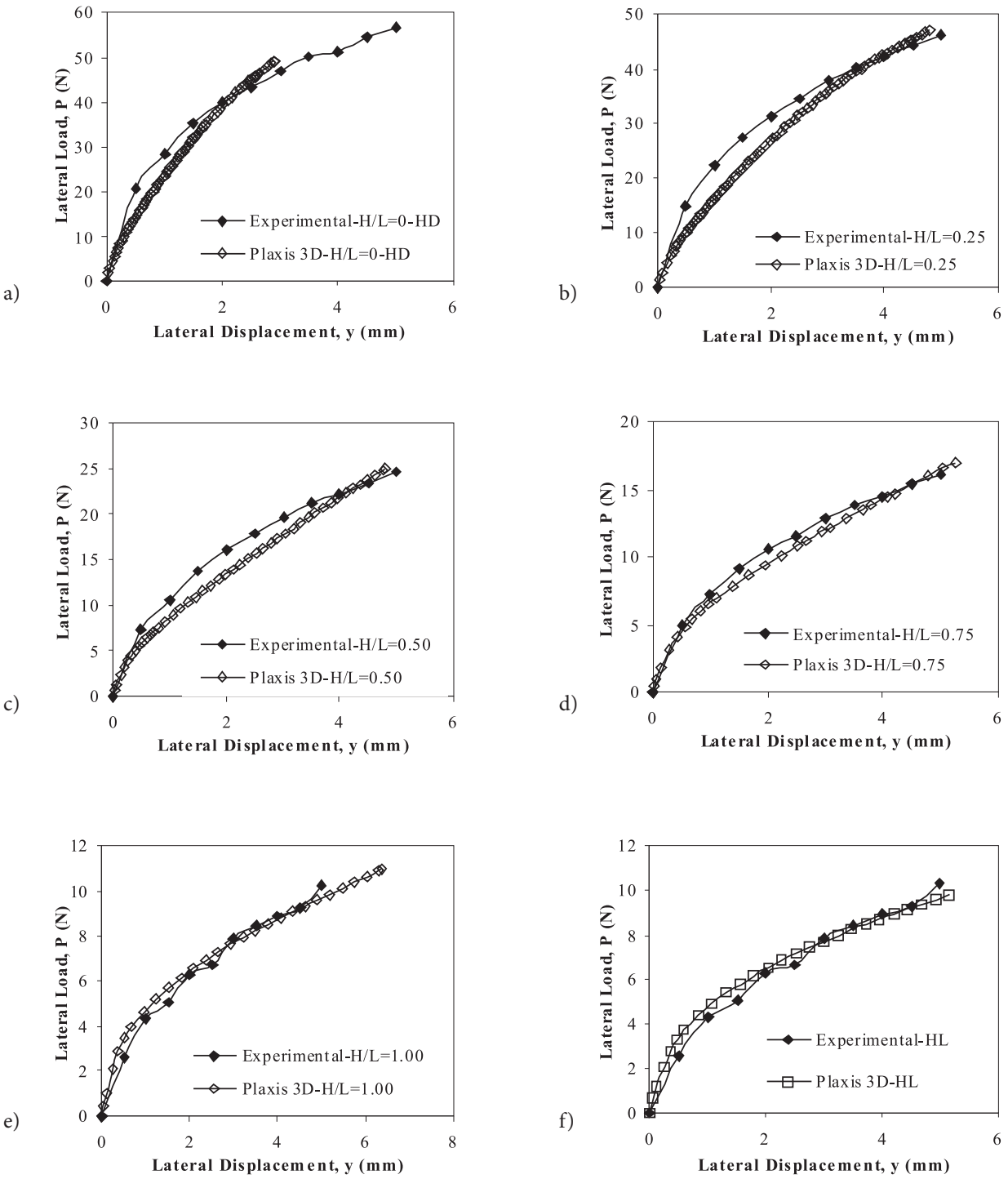

Figure 15. The lateral load-displacement relations at the pile head.

the system could be considered under the experimental conditions.

The lateral load-displacement relations at the pile head obtained from the experimental model studies and numerical analyses are compared in Fig. 15 for the cases of H/L=0 (Homogeneous dense sand condition), 0.25, 0.50, 0.75, 1.00 and the homogeneous loose sand condition, respectively. Since the tip resistance of the pile was neglected in the calculations, the homogeneous loose sand condition may

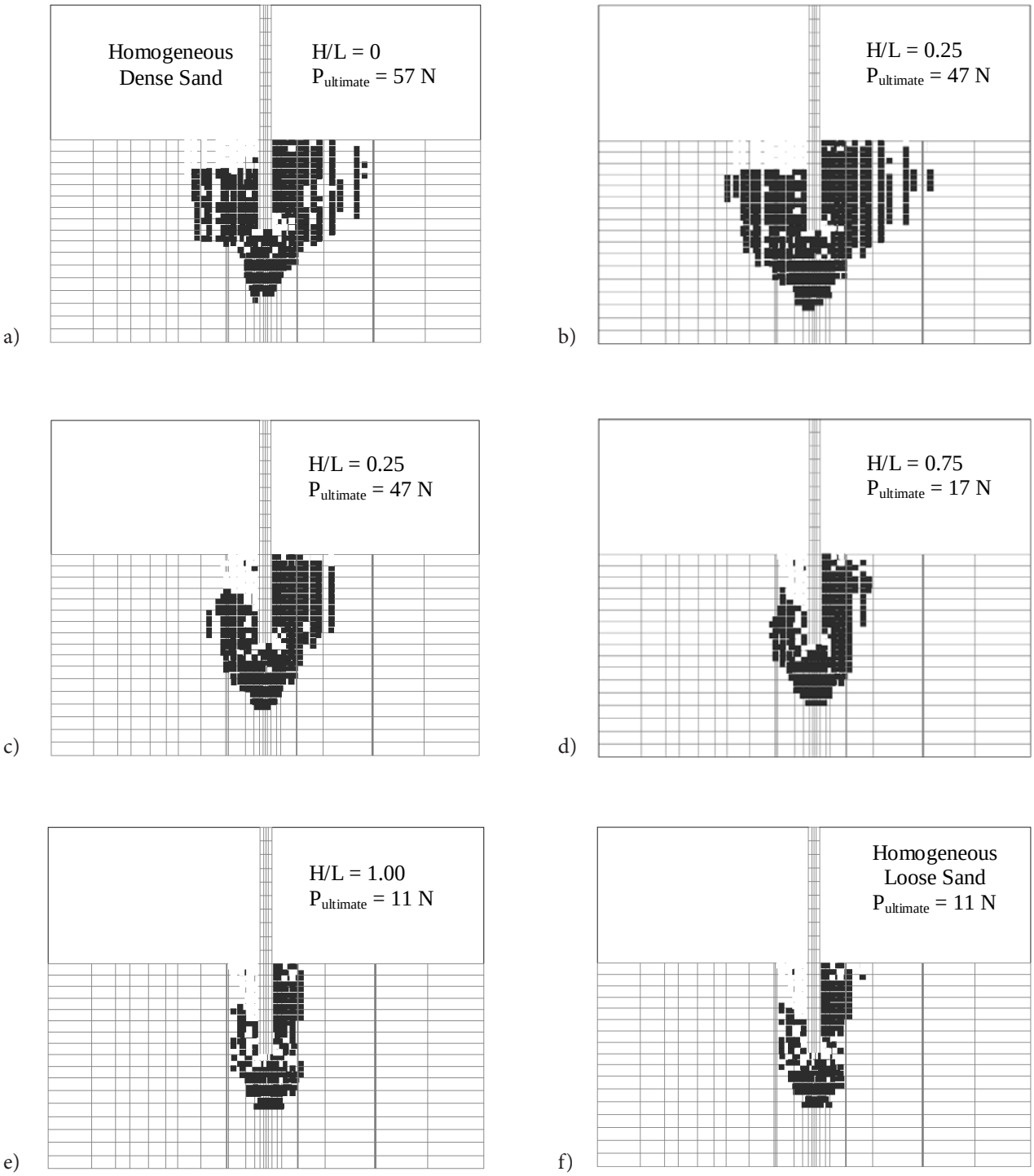

Figure 16. The failure regions developed around the pile.

be assumed as H/L=1. The results obtained from numerical analyses performed in the homogeneous loose sand and in the case of H/L=1 also confirm this assumption.

As seen in Fig. 15, in general, a very good agreement between the curves, especially for the cases of H/L=0.75, H/L=1.00 and homogeneous loose sand condition, was observed. The relationships between the lateral load and lateral displacement obtained from both experimental and numerical studies are non-linear in all the cases considered. As shown in Fig. 15 (a), in the analysis performed in the homogeneous dense sand condition, failure occurred at any loading step during the analysis and no peak lateral resistance was observed. This might be due to an associated flow rule when a strain hardening soil response was used. A more realistic analysis could be performed using a non-associated flow rule with strain softening and the reduction from peak to critical state friction angles could be taken into account as a function of plastic strains. It is clear that the void ratio extent of the soil will be smaller and the soil will be more compact and dense when the value of H/L decreases. If the lateral loads corresponding to the same lateral displacement in each of the soil conditions are compared, it can be concluded that the range in which the soil behaves elastically will be greater with decreasing thickness of the upper loose sand layer.

In the case of a short rigid pile the failure occurs as the lateral earth pressures reach the ultimate passive lateral resistance of the soil along the pile length. The pile rotates around a point somewhere along its length and causes the development of a passive resistance in the soil in front of the pile above the rotation point and the back side of the pile below the rotation point. Once the mobilizing passive resistance is equal to the limit state of the passive earth pressure, failure takes place and then a further displacement of the pile does not significantly effect the passive pressure. This phenomenon is well simulated by the non-linear 3D FE analyses.

The calculated failure regions when the pile head reaches the lateral displacement of 5 mm under the lateral load are depicted in Fig. 16. The failure regions are composed of plastic stress (shear yielding) points. Plastic stress point can be either a mohr-coulomb point or a tension cut-off point. The Mohr-Coulomb points shown in the figure with a black color represent the mobilizing passive resistance in the sand. On the other hand, the white regions consist of tension cut-off points represent the mobilizing active pressure. As expected, the mohr-coulomb points develop not only in the sand in front of the pile above the rotation point but also at the back side and bottom. Similarly, the tension cut-off points develop not only in sand at the back side of the pile above the rotation point near the sand surface but also in front of the pile below the rotation point near the pile tip.

Although the failure zone that occurred in the case of H/L=0.25 is a litttle greater than the failure zone in the case of H/L=0, the ultimate lateral load capacity of the pile in the case of H/L=0.25 is nearly 19% smaller than that obtained in the case of H/L=0. The rotation points in the cases of H/L=0 and H/L=0.25 are almost at the same depths. Therefore, the passive resistances developed below the rotation point will be equal for these two cases. The difference between the ultimate lateral load capacities is due to the upper loose sand layer in the case of H/L=0.25. This is because the shallow zone close to the sand surface could not provide a contribution to the lateral resistance as well as in the case of H/L=0.

As seen in Fig. 16, the boundaries of the failure regions extend to greater depths and greater lateral distances with the decreasing thickness of the upper loose sand layer. However, the lateral load capacity of the pile in the layered sand condition is significantly affected by the length of the pile within the dense sand layer. In the case of H/L=0, the failure zone propagates to a lateral distance approximately five times that of the pile diameter from the front of the pile, while these distances are approximately 4D and 3D from the back side and the bottom, respectively. The distances of the failure regions from the in front, rear and tip of the pile for each of the soil conditions are summarized in Table 9. It is apparent from Fig. 16 that the relative density has a major effect on the lateral load capacity of short rigid piles.

In order to predict the ultimate lateral load capacity ($P_{ultimate}$) of short rigid piles it is necessary to know the distribution of the lateral effective stresses mobilized along the pile embedded length. Thus, the unknown value of $P_{ultimate}$ can be determined from the equilibrium

Table 9. The distances of the failure regions from the in front, rear and tip of the pile.

	$HD = H/L$=0	H/L = 0.25	H/L = 0.50	H/L = 0.75	H/L = 1.00	$HL=H/L$=1
Front	4D ~ 5D	4D ~ 5D	3D	2D	D	D
Rare	4D	4D	2D	D	D	D
Tip	3D	3D	3D	2D	2D	2D

condition of the horizontal forces acting on the pile and the moments calculated according to a point defined. The lateral effective stress (σ'_h) is an important factor affecting significantly the $P_{ultimate}$ values [39].

Brinch Hansen [12] presented a method to predict the lateral load capacity of short rigid piles in a general c-ϕ soil, where c and ϕ' are the cohesion and the effective internal friction angle of the soil, respectively. Brinch Hansen [12] proposed an empirical formula from which the depth of the rotation point is determined by means of trial and error. The passive lateral earth pressure areas developed above and below the rotation point yield equal moments at the point where the lateral load is applied. The difference between the two pressure areas gives the lateral load capacity of a short rigid pile subjected to a lateral load. The ultimate lateral resistance of cohesionless soil, $P_{ultimate}$, per unit length of the pile at a depth of z is calculated using the following equation:

$$P_{ultimate} = p_z \; K_{qz} \; D \qquad (12)$$

where:

p_z ; effective overburden pressure at a depth of z,
K_{qz} ; earth pressure coefficient which is a function of the pile diameter and friction angle,
D ; diameter of the pile.

Meyerhof et al. [14] proposed a method to estimate the lateral load capacity of short rigid piles founded in two-layered soil deposits. This method calculates the ultimate lateral load capacity of the pile assuming that the variation of lateral effective stresses with depth is linear. The three-dimensional characteristic of the lateral soil resistance is taken into account using shape factors. In this method, the depth to the pile rotation point is determined by solving the equations obtained from the equilibrium condition of the resultant horizontal forces and moments. Meyerhof et al. [14] suggested the following relationship to define the lateral load capacity of short rigid piles in layered sand.

$$Q_U = D \left(\gamma \, L^2 \, K_b \, F_b \, r_b \, s_b \right) \qquad (13)$$

where:

D : pile diameter,
γ : average value of the unit weights of the sand layers,
L : embedded length of the pile,
K_b : net earth pressure coefficient defined as $K_b = [\tan2(45+\phi/2) - \tan2(45-\phi/2)]$,
F_b : lateral resistance factor defined corresponding to the ratio of K_{b1} / K_{b2},
r_b : moment reduction factor defined as $r_b = 1 / (1 + 1.4e / D)$,
s_b : shape factor which is dependent on H/L, ϕ' and L/D,
e : load eccentricity.

The value of the lateral effective stress at a depth of z is calculated using the following equation:

$$\sigma'_h = \gamma \, z \, K_b \, s_b \qquad (14)$$

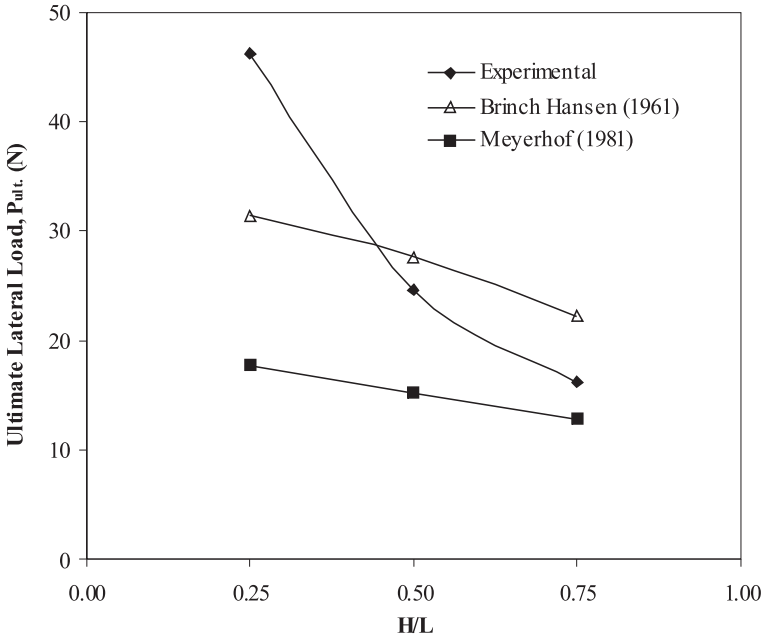

Figure 17. The comparison of the lateral load capacities with respect to H/L.

The ultimate lateral load capacities obtained for the cases of H/L=0.25, 0.50 and 0.75 from the method suggested by Brinch Hansen [12] and Meyerhof et al. [14] and model test studies are compared in Fig. 17. Also, the distributions of the lateral effective stresses along the pile embedded depth obtained from the methods proposed by Brinch Hansen [12] and Meyerhof et al. [14] and 3D non-linear FE analyses for the case of H/L=0.25 are shown in Fig. 18. Since the 3D FE analysis was carried out under the experimental lateral load level, the lateral effective stresses developed under the experimental loading level have been obtained.

As shown in Fig. 17, the lateral load capacities obtained from both methods proposed by Brinch Hansen [12] and Meyerhof et al. [14] and model test studies decrease with the increasing value of the H/L ratio. The reduction in the values of the ultimate lateral load capacities with respect to the H/L ratio is non-linear for the experimental results, while it is approximately linear for the values obtained from the methods suggested by Brinch Hansen [12] and Meyerhof et al. [14]. The difference between the two ultimate lateral load capacity ($P_{ultimate}$) values obtained from Brinch Hansen's method and the experimental study for the case of H/L=0.25 is approximately as well as the 30% of the experimental capacity, while this ratio is equal to 60% of the experimental capacity for the Meyerhof et al.'s method. Brinch Hansen's [12] method overestimates the $P_{ultimate}$ values with respect to the experimental results for the cases of H/L=0.50 and H/L=0.75. The $P_{ultimate}$ values differ as the ratio of 10% and 40% of the $P_{ultimate}$ values observed in the experimental studies for the H/L=0.50 and H/L=0.75, respectively. The method suggested by Meyerhof et al. [14] underestimates the $P_{ultimate}$ values with respect to the experimental values in all of the combinations of the layered sand profile considered. The differences between two $P_{ultimate}$ values are the 37% and 20% of the experimental $P_{ultimate}$ value for the cases of H/L=0.50 and H/L=0.75, respectively. The ultimate lateral load capacities, in all three cases (i.e., H/L=0.25, H/L=0.50 and H/L=0.75), calculated using the Brinch Hansen's [12] method are approximately equal to 1.75 times the load-capacity values predicted from the method proposed by Meyerhof et al. [14].

Fig. 18 shows the distribution of the lateral effective stresses along the pile embedded length for the case of H/L=0.25. The distributions of the lateral effective stresses predicted from the methods proposed by Brinch Hansen [12] and Meyerhof et al. [14] are linear through the upper and lower sand layers. In these methods the maximum lateral effective stresses occur at the depth of rotation point in front of the pile. The depths of the rotation points were calculated as the depths equal to 77% and 67% of the embedded pile length for the methods of Brinch Hansen [12] and Meyerhof et al. [14], respectively. In the FE analysis, the value of the lateral effective stress is zero at the depth of the rotation point and has a maximum value at an average depth corresponding to 50% of the embedded pile length below the sand surface. On the back side of the pile below the rotation point, maximum pressure is developed at the vicinity of the pile tip. This result is in line with the conventional methods used in comparison.

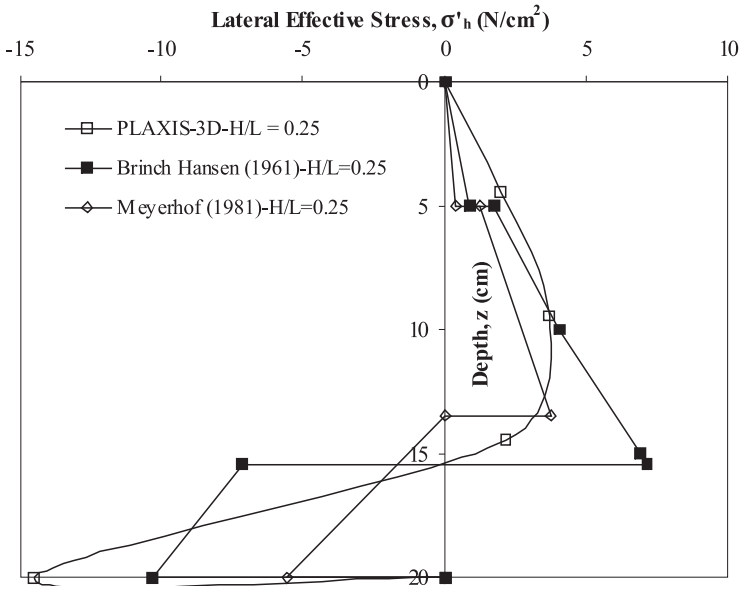

Figure 18. The distributions of the lateral effective stresses along the pile length.

The distribution of the lateral effective stresses computed by PLAXIS is non-linear through the layered sand profile. The rotation point is located at an average depth corresponding to 86% of the embedded pile length.

The discrepancies between the results of the conventional methods and among the conventional methods and model test studies and among the conventional methods and non-linear FE analysis could be attributed to the three-dimensional effect of the laterally loaded pile problem and selected distribution form in the conventional method for the lateral effective stresses. The conventional methods used in comparison adopt different expressions of lateral soil resistance with a differently assumed distribution of lateral soil pressure with depth. Conventional methods assume that the distribution of lateral effective stresses with depth is linear. On the other hand, in both homogeneous and layered sand conditions, the variation of the lateral effective stresses with depth would be non-linear. The value of the ultimate lateral load capacity could be significantly different, depending on the methods used. The three-dimensional effect of the problem is taken into account using a shape factor in the conventional method. However, in the FE method, 3D stress state can be taken into account and the problem can be considered as a whole in 3D space.

The base shear resistance, Q_b, for sand can be calculated using the equation given below [40].

$$Q_b = \frac{p}{4} D^2 s_b \tan d_b \qquad (15)$$

where:

σ_b is the overburden pressure at the pile tip,
δ_b is the friction angle at the interface of the pile tip and soil (in this study, δ_b has been calculated as $\tan \delta_b = R_{inter} \tan \phi_{soil}$).

In the layered sand conditions, the parameters of eq. 15 such as the D and δ_b are the same for all cases since the model pile with 50 mm diameter was used in all of the analyses. The pile tip was located on the dense sand in all the cases considered. Therefore, eq.15 returns to the following form.

$$Q_b = 2.464\ \sigma_b \qquad (16)$$

Almost the same average values were calculated for the overburden pressure as equal to 0.33, 0.32 and 0.31 N/cm^2 for the cases of H/L=0.25, 0.50 and 0.75, respectively. The base resistance calculated at the pile tip in the case of H/L=0.25 is equal to 1.72% of the ultimate lateral load capacity. This ratio has been obtained as 3.14% and 4.47% for the cases of H/L=0.50 and 0.75, respectively.

For short rigid piles, the base shear resistance can be significant provided that an adequate horizontal movement occurs at the pile tip. The lateral displacements observed at the pile tip were equal to 1.45% of the pile diameter for the case of H/L=0.25 and 0.60% and 0.33% for the cases of H/L=0.50 and 0.75, respectively. In layered sand conditions, the depth of the rotation point moves toward the pile tip with the increasing thickness of the loose sand layer. As a result, the lateral displacement at the pile tip and therefore the contribution of the base resistance decreases. The calculated mobilized shear strength values when the pile head reaches the lateral displacement of 5 mm under lateral load in the case of H/L=0.25 are illustrated in Fig. 19. On the other hand, the vertical load and interface behavior and also the factors affecting the base resistance contribution. There is no vertical load applied to the pile except the self-weight of the model pile and pulling arm. Since the horizontal movement of the pile tip is insufficient for the fully mobilized base resistance it was ignored in the calculations. The tip resistance of the pile was assumed to have a small contribution to the overall lateral load capacity.

O' Neill pointed out that in large-drilled shafts, the push-pull resistance provided by the vertical side shear resistance occurred due to the rotation of the pile can resist partially the moment at the pile head. The effect of the push-pull resistance can be significant especially in rocks [41]. Yang [40] proposed a method based on parametric study results to estimate the push-pull resistance of short drilled shafts. In the proposed method, the dominant factor affecting the push-pull moment resistance is the coefficient of friction of the shaft-sand interface and the push-pull moment resistance increases linearly with the coefficient of friction of the interface. In the present study, the embedded model pile was used. The surface of the pile was smooth. The model soil was dry, uniform and poorly graded sand. Depending on these factors the values of the coefficient of friction of the pile-sand interface used in the analyses of the model tests obtained were too small considering the values of the interface friction coefficient used in the analyses of in-situ conditions. Both in the experimental studies and numerical analyses, it was observed that the depth of the rotation point in layered sand conditions moves toward the pile tip with increasing depth of the loose sand layer. As a result, the push-pull resistance of the pile will reduce because of the decreasing length of the push zone and coefficient of friction between the pile and sand. The push-pull moment values calculated using the method proposed by Yang [40] in loose and dense sand conditions were assumed as having small contributions to resist the moment at the pile head and therefore it was neglected evaluating the results.

a)

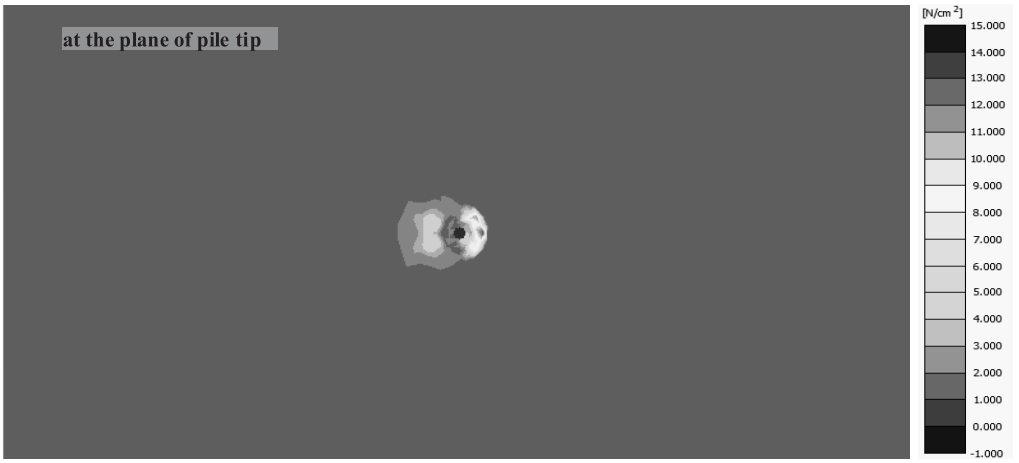

b)

Figure 19. The distributions of the mobilized shear strengths at the ultimate condition in the case of H/L=0.25: a) along the pile embedment length, b) across the base of the pile.

8 LIMITATIONS

Full-scale loading test results are valid especially for in-situ conditions and for soil properties in which the test was performed. However, a full-scale loading test is not economic due to the expensive cost in time and money required for construction, instrumentation and testing. Therefore, small-scale model test studies are used widely as an alternative to full-scale loading tests. It is well recognized that small-scale model test studies carried out in cohesionless soils involve a scale-error [7, 31, 42].

In the present study, the model tests were conducted on 1/20-scale model piles, while the used sand particles were the same dimensions as in the prototype.

There are several recommendations related to the scale effect in the literature. Franke and Mutt [43] suggested that the scale-error can be neglected when the ratio of the pile diameter to the mean grain size is greater than 30. On the other hand, Ovesen [44] proposed that the ratio of the pile circumference to grain size should be in excess of 15-30 to avoid the scale effects. In the present study, the relationships between the dimensions of the model pile diameter and sand particle size satisfy the two recommendations mentioned above.

Despite all of these, this study should be evaluated a useful basis for further research and the results of this study should be supported with full-scale loading tests or centrifugal model test studies.

9 CONCLUSIONS

The behavior of short rigid piles subjected to a lateral load in two-layer sand deposits of different densities and thicknesses was investigated through model test studies and three-dimensional non-linear FE analyses. However, a parametric study was also performed to investigate the effects of the elasticity modulus of sand, sand dilatancy and interface behavior on the lateral load capacity of short rigid piles. Additionally, the lateral load capacities and the distribution of the lateral effective stresses were calculated using the methods proposed by Brinch Hansen [12] and Meyerhof et al. [14]. The results obtained from model test studies, numerical analyses and conventional methods were compared with each other. Based on the investigations the following main conclusions can be drawn.

- The soil packing effects the lateral load capacity of short rigid piles markedly. The lateral load capacity of the pile in homogeneous dense sand is approximately five times that in homogeneous loose sand.
- The lateral load capacities obtained in the layered sand conditions decrease non-linearly as the thickness of the upper loose sand layer increases. The reduction is mainly due to the smaller unit weight and lower stiffness of the upper loose sand layer.
- The lateral displacement observed at the pile head decreases due to a stiffer surface layer with the increasing value of $E_{reference}$.
- The volume of the sand mass mobilized under the lateral load will be more in the case of higher dilatation values. As a result, higher dilatation values will provide greater lateral load capacities and smaller lateral displacements.
- The interface behavior is significantly dependent on sand density. The degree of permanent slipping behavior between the pile and sand surfaces decreases depending on the decreasing value of R_{inter}.
- Failure zones developed around the pile propagate greater lateral distances and greater depths with the decreasing thickness of the upper loose sand layer.
- The laterally loaded pile problem has been modeled satisfactorily using a three-dimensional non-linear finite-element method.
- Contrary to the assumption made by conventional methods, the distribution of the lateral effective stresses is not linear along the pile embedded depth. The method suggested by Meyerhof et al. [14] produces very conservative lateral load capacities in the layered sand conditions considered.
- The value of the ultimate lateral load capacity could be significantly different depending on the methods used.

ACKNOWLEDGMENTS

The authors thank the Cukurova University Scientific Research Project Directorate for supporting this study (Project no: MMF2006D2).

REFERENCES

[1] Fan, C.C. and Long, J.H. (2005). Assessment of existing methods for predicting soil response of laterally loaded piles in sand. *Computers and Geotechnics*, 32, 274-289.

[2] Johnson, K., Lemcke, P., Karunasena, W. and Sivakugan, N. (2006). Modelling the load-deformation response of deep foundations under oblique loading. *Environmental Modelling and Sofware*, 21, 1375-1380.

[3] Shen, C.K., Bang, S., Desalvatore, M. and Poran, C.J. (1988). Laterally Loaded Cast-in-Drilled-Hole Piles. *Transportation Research Record*, 1191, 155-165.

[4] Nazir, R. (1994). *The moment-carrying capacity of short piles in sand*. Ph.D. thesis, University of Liverpool, U.K.

[5] Laman, M. (1995). *The moment carrying capacity of short pier foundations in clay*. Ph.D. thesis, University of Liverpool, U.K.

[6] King, G.J.W. and Laman, M. (1995). Conventional and centrifuge model studies of the moment-carrying capacity of short pier foundation in clay. *Canadian Geotechnical Journal*, 32, 976-988.

[7] Dickin, E.A. and Nazir, R. (1999). Moment-carrying capacity of short pile foundations in cohesionless soil. *Journal of Geotechnical and Geoenvironmental Engineering*, ASCE, 125 (1), 1–10.

[8] Dickin, E.A. and Laman, M. (2003). Moment response of short rectangular piers in sand. *Computers and Structures*, 81, 2717-2729.

[9] Chae, K.S., Ugai, K. and Wakai, A. (2004). Lateral resistance of short single piles and pile groups located near slopes. *International Journal of Geomechanics*, 4(2), 93-103.

[10] Hu, Z., McVay, M., Bloomquist, D., Herrera, R. and Lai, P. (2006). Influence of torque on lateral capacity of drilled shafts in sands. *Journal of Geotechnical and Geoenvironmental Engineering*, ASCE, 132 (4), 456-464.

[11] Lee, S.W., Pickles, A.R. and Henderson, T.O. (2006). Numerical modeling of laterally loaded short pile. *Numerical Methods in Geotechnical Enginnering-Schweiger (ed.)*. Taylor&Francis Group, London.

[12] Brinch-Hansen, J. (1961). The ultimate resistance of rigid piles against transversal forces. *Geoteknisk Institut (The Danish Geotechnical Institute)*, Bulletin No. 12, 5-9.

[13] Broms, B.B. (1964). Lateral resistance of piles in cohesionless soils. J*ournal of Soil Mechanics and Foundations Division, ASCE*, 90 (3), 123-156.

[14] Meyerhof, G.G., Mathur, S.K. and Valsangkar, A.J. (1981). Lateral resistance and deflection of rigid walls and piles in layered soils. *Canadian Geotechnical Journal*, 18, 159-170.

[15] Prasad, Y.V.S.N. and Chari, T.R. (1999). Lateral capacity of model rigid piles in cohesionless soils. *Soils and Foundations*, 39 (2), 21-29.

[16] Zhang, L., Silva, F. and Grismala, R. (2005). Ultimate lateral resistance to piles in cohesionless soils. *Journal of Geotechnical and Geoenvironmental Engineering, ASCE*, 131 (1), 78-83.

[17] Muqtadir, A. and Desai, C.S. (1986). Three-dimensional analysis of a pile-group foundation. *International Journal for Numerical and Analytical Methods in Geomechanics*, 10, 41-58.

[18] Brown, D.A. and Shie, C.F. (1990). Three-dimensional finite element model of laterally loaded piles. *Compututers and Geotechnics*, 10, 59-79.

[19] Trochanis, A.M., Bielak, J. and Christiano, P. (1991). Three-dimensional nonlinear study of piles. *Journal of Geotechnical Engineering, ASCE*, 117 (3), 429–447.

[20] Wakai, A., Gose, S. and Ugai, K. (1999). 3-D Elasto-plastic finite element analyses of pile foundations subjected to lateral loading. *Soils and Foundations*, 39(1), 97-111.

[21] Yang, Z. and Jeremic, B. (2003). Numerical study of group effects for pile groups in sands. *International Journal for Numerical and Analytical Methods in Geomechanics*, 27, 1255-1276.

[22] Martin, G.R. and Chen, C.Y. (2005). Response of piles due to lateral slope movement. *Computers and Structures*, 83, 588-598.

[23] Karthigeyan, S., Ramakrishna, V.V.G.S.T. and Rajagopal, K. (2006). Influence of vertical load on the lateral response of piles in sand. *Computers and Geotechnics*, 33, 121-131.

[24] Karthigeyan, S., Ramakrishna, V.V.G.S.T. and Rajagopal, K. (2007). Numerical investigation of the effect of vertical load on the lateral response of piles. *Journal of Geotechnical and Geoenvironmental Engineering, ASCE*, 133 (5), 512-521.

[25] Yang, Z. and Jeremic, B. (2005). Study of soil layering effects on lateral loading behavior of piles. *Journal of Geotechnical and Geoenvironmental Engineering, ASCE*, 131 (6), 762-770.

[26] Yang, K. and Liang, R. (2006). Numerical solution for laterally loaded piles in a two-layer soil profile. *Journal of Geotechnical and Geoenvironmental Engineering*, 132 (11), 1436-1143.

[27] Avaei, A., Ghotbi, A.R. and Aryafar, M. (2008). Investigation of pile-soil interaction subjected to lateral loads in layered soils. *American Journal of Engineering and Applied Sciences*, 1 (1), 76-81.

[28] Czerniak, E. (1957). Resistance to overturning of single, short piles. *Journal of the Structural Division, Proceedings of the American Society of Civil Engineers*, 83 (2),1188, 1-25.

[29] Terzaghi, K. (1955). Evaluation of coefficients of subgrade reaction. *Geotechnique*, 5(4), 297-326.

[30] El Naggar, M.H. and Wei, J.Q.(1999). Response of tapered piles subjected to lateral loading. *Canadian Geotechnical Journal*, 36, 52-71.

[31] Sawwaf, M.E. (2006). Lateral resistance of single pile located near geosynthetic reinforced slope. *Journal of Geotechnical and Geoenvironmental Engineering*, 132 (10), 1336-1345.

[32] Zienkiewicz, R.F. and Taylor, R.L. (1994). *The finite element method (4th edn)*. McGraw-Hill, London, U.K.

[33] Bolton, M.D. (1986). The strength and dilatancy of sands. *Geotechnique*, 36(1), 65-78.

[34] Laman, M., King, G.J.W. and Dickin, E.A. (1999). Three-dimensional finite element studies of the moment-carrying capacity of short pier foundations in cohesionless soil. *Computers and Geotechnics*, 25, 141-155.

[35] Jaky, J. (1944). The coefficient of earth pressure at rest. *Journal for Society Hungarian Architects and Engineers*, 78, 355-358.

[36] Maeda, K. and Miura, K. (1999). Confining stress dependency of mechanical properties of sands. *Soils and Foundations*, 39 (1), 53-67.

[37] Matlock, H. and Reese, L.C. (1960). Generalized solutions for laterally loaded piles. *Journal of Soil Mechanics and Foundations Division, ASCE*, 86 (5), 63-91.

[38] Ng, P.C.F., Pyrah, I.C. and Anderson, W.F. (1997). Assesment of the interface elements and modification of the interface element in CRISP90. *Computers and Geotechnics*, 21 (4), 315-339.

[39] Lee, J., Kim, M. and Kyung, D. (2010). Estimation of lateral load capacity of rigid short piles in sands using CPT results. *Journal of Geotechnical and Geoenvironmental Engineering, ASCE*, 136 (1), 48-56.

[40] Yang, K. (2005). Lateral capacity of drilled-shafts considering push-pull resistance. *Proceedings of Deep Foundations Institute 30th Annual Conference on Deep Foundations,* Chicago, IL, 527-536.

[41] Reese, L.C. (1997). Analysis of laterally loaded piles in weak rock. *Journal of Geotechnical and Geoenvironmental Engineering, ASCE*, 123 (11), 1010-1017.

[42] Hameed, R.A., Gunaratne, M., Putcha, S., Kuo, C. and Johnson, S. (2000). Lateral load behavior of jetted piles. *Geotechnical Testing Journal*, 23 (3), 358-368.

[43] Franke, E. and Muth, G. (1985). Scale effect in 1g model tests on horizontally loaded piles. *Proceedings of the 11th International Conference of Soil Mechanics and Foundation Engineering*. San Fransisco, 2, 1011-1014.

[44] Ovesen, N.K. (1979). The use of physical models in design: the scaling law relationship. *Proceedings of the 7th European Conference on Soil Mechanics and Foundation Engineering*. 4, 318-323.